Hydrothermal synthesis of highly stable CuO nanostructures for efficient photocatalytic degradation of organic dyes

Article *in* Materials Science in Semiconductor Processing · February 2015

DOI: 10.1016/j.mssp.2014.10.012

CITATIONS
15

READS
205

6 authors, including:

Sonia S
Holy Cross College (Autonomous), Nagercoil
9 PUBLICATIONS **54** CITATIONS
SEE PROFILE

Palaniswamy Suresh Kumar
Center of Innovation, Singapore
64 PUBLICATIONS **1,713** CITATIONS
SEE PROFILE

Ponpandian Nagamony
Bharathiar University
117 PUBLICATIONS **2,595** CITATIONS
SEE PROFILE

Chinnuswamy Viswanathan
Bharathiar University
61 PUBLICATIONS **565** CITATIONS
SEE PROFILE

Materials Science in Semiconductor Processing 30 (2015) 585–591

Contents lists available at ScienceDirect

Materials Science in Semiconductor Processing

journal homepage: www.elsevier.com/locate/mssp

Hydrothermal synthesis of highly stable CuO nanostructures for efficient photocatalytic degradation of organic dyes

S. Sonia [a], S. Poongodi [a], P. Suresh Kumar [b], D. Mangalaraj [a,*], N. Ponpandian [a], C. Viswanathan [a]

[a] Department of Nanoscience and Technology, Bharathiar University, Coimbatore 641046, India
[b] Thin Film and Nanomaterials Laboratory, Department of Physics, Bharathiar University, Coimbatore 641046, India

ARTICLE INFO

Available online 22 November 2014

Keywords:
CuO
Nanoleaves
Hydrothermal
Optical properties
Photocatalytic

ABSTRACT

Highly stable CuO nanoleaves were synthesized by a simple hydrothermal method using tri-sodium citrate as a structure directing agent. The surface shape of the CuO nanoleaves was controlled and optimized by adjusting the molar concentration of the citrate. The structural properties of the prepared nanoleaves were investigated using X-ray diffraction which confirmed the formation of monoclinic CuO with an average crystallite size of 13–17 nm. FESEM and TEM analysis techniques confirmed the leaf-like morphology of CuO with sizes ranging from 250–300 nm. Analysis of the SAED pattern showed the polycrystalline nature of CuO nanoleaves. The band gap energy E_g was evaluated as ranging from 2.67 to 2.97 eV from the UV–visible spectrum. CuO nanoleaves exhibited excellent recyclable photocatalytic activity with degradation values of 89% and 96% for methylene blue (MB) and methylene violet (MV) dyes respectively under ultraviolet light illumination. Thus, the present work is significant in terms of the potential applications in waste water treatment.

1. Introduction

Recently, metal oxide nanostructures have attracted great attention in the field of photocatalysis to degrade the organic compounds present in contaminated water. This heterogeneous photocatalysis route leads to the complete degradation of organic pollutants through their interaction with the photogenerated charge carriers and reactive oxygen species [1]. As a heterogeneous catalyst, tenorite (CuO) has been used for the conversion of hydrocarbons into carbon dioxide and water and also for catalytic oxidation of cyclohexane and oxidative degradation of methylene blue in waste water [2–4]. Apart from the widely used photocatalysts such as TiO_2 and ZnO [5–7], p-type semiconductor CuO has been employed as an effective photocatalyst due to its high photochemical stability [8–10]. Even though CuO has been publicized as a good photocatalyst in many reports [11,12], its photocatalytic properties for the degradation of pollutants are directly related to the synthesis route, particle size and shape. Hence, a study of the synthesis and applications of CuO is both theoretically and practically important.

In recent years, efforts have been made to synthesize a variety of well-defined CuO nanostructures such as nanoflowers, hollow spheres, nanodendrites, and nanorods by various wet chemical methods [13–16]. Among them, the hydrothermal process has been considered as the most promising route for the controlled synthesis of CuO nanostructures due to its simplicity and other advantages

* Corresponding author. Tel.: +91 422 2425458; fax: +91 422 2422387.
E-mail address: dmraj800@yahoo.com (D. Mangalaraj).

http://dx.doi.org/10.1016/j.mssp.2014.10.012
1369-8001/

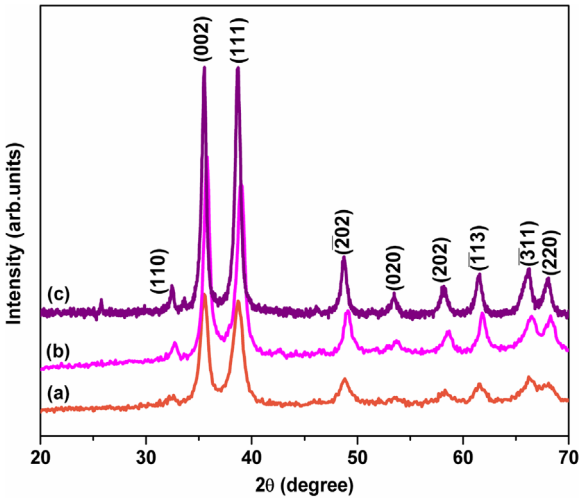

Fig. 1. XRD spectra of copper oxide (CuO) nanoleaves: (a) without sodium citrate, (b) with 0.05 M sodium citrate and (c) with 0.1 M sodium citrate.

such as low temperature required, and the potential for large scale production. Generally, sodium citrate (SC) is employed as a reducing agent in the synthesis of noble metals [17] and also serves as a shape controller and stabilizing agent in the synthesis of hexagonal ZnO microrods and CuO nanorods [18,19]. Herein, we report a simple hydrothermal route for the preparation of highly stable CuO nanoleaves with increased surface area in the presence of sodium citrate and its photocatalytic action on organic pollutants such as methylene blue and methylene violet has been investigated. In order to examine the stability of the CuO catalyst, a recycling experiment was carried out.

2. Experiment

2.1. Synthesis of CuO nanoleaves

Nanostructured CuO nanoleaves were prepared by the simple hydrothermal method. In a typical reaction process, 0.1 M of copper acetate dehydrate (HIMEDIA, 99%, AR grade) was dissolved in double distilled water (50 ml) after which, 50 ml of 1 M aqueous solution of NaOH (SDFCL, 97%, LR grade) was added dropwise into the above solution under stirring. Further, tri-sodium citrate (SDFCL, 99.0–100.5%, LR grade) was introduced into the above mixture under continuous stirring at different molar concentrations (0.05 M and 0.1 M). The resultant solution was then transferred into Teflon lined stainless steel autoclaves, sealed and maintained at 160 °C for 12 h. Finally, the obtained black colored precipitate was washed with distilled water and ethanol and dried at 80 °C for 2 h.

2.2. Material characterizations

A PAN analytical (X-Pert-Pro) X-ray diffractometer using Cu Kα1 radiation ($\lambda = 1.5406$ Å) was employed to analyze the crystallographic properties of the CuO nanorods. The surface morphologies were studied by a FEI Quanta-250 Field Emission Scanning Electron Microscopy (FESEM). UV–vis spectrum was recorded on a Jasco V-650 spectrophotometer. The TEM image and selected area electron diffraction (SAED) pattern were recorded using a 120 KV Tecnai Sprit TEM instrument. The specific surface area was calculated with the Brunauer–Emmett–Teller (BET) equation, and the pore size distribution was calculated from the adsorption curve by the Barrett–Joyner–Halenda (BJH) method.

2.3. Photocatalysis test

Methylene blue (MB) and methylene violet (MV) (HIMEDIA, practical grade) were chosen as the organic pollutants to evaluate the photocatalytic performance of CuO nanoleaves. In a typical experiment, 5 mg of the catalyst (CuO) was dispersed in 100 ml of aqueous solutions (15 mg/L) of MB and MV. The solutions were stirred in darkness to establish adsorption/desorption equilibrium between the catalyst and the dye molecules. The solutions were then illuminated by an UV source ($\lambda_{max} = 365$ nm) to induce photochemical reaction. The samples were collected at intervals of 30 min and the concentration values of the dye solutions were determined using a UV–vis spectrophotometer (Jasco-V-650).

3. Results and discussion

3.1. Structural analysis

The phase purity of CuO nanoleaves was determined by powder X-ray diffraction (XRD) as shown in Fig. 1a–c. Diffraction peaks along (110), (111), (111), (202) and (020) planes confirm the monoclinic structure of CuO with a single phase which is consistent with the standard data (JCPDS PDF Card no. 05-0661). The absence of copper hydroxide phase confirms that the tenorite could be directly obtained in this process without any calcination step for phase transformation, one of the advantages of the hydrothermal process [20]. The broadening of all the diffraction peaks in the XRD pattern indicates that the component crystallites are of nanoscale character. No other impurities were detected by XRD analysis, indicating the phase purity of the CuO nanoleaves, which was consistent with the results of the EDS analysis (Fig. 2d). The average grain size of copper oxide nanoleaves was calculated by using the Scherrer formula ($D = 0.89\lambda/\beta\cos\theta$), where D is the crystallite size, λ is the wavelength (1.5406 Å for Cu Kα), β is the full-width at half-maximum (FWHM) of the main intensity peak after subtraction of the equipment broadening and θ is the diffraction angle. The calculated average crystallite size obtained by using the (111) planes of CuO ranged from 13 to 17 nm for the samples prepared with and without citrate.

3.2. Morphological analysis

The morphology of the CuO prepared with and without sodium citrate was observed via a field emission scanning electron microscope (FESEM) and is shown in Fig. 2a–c. Fig. 2a shows aggregated seed-like CuO nanostructures of

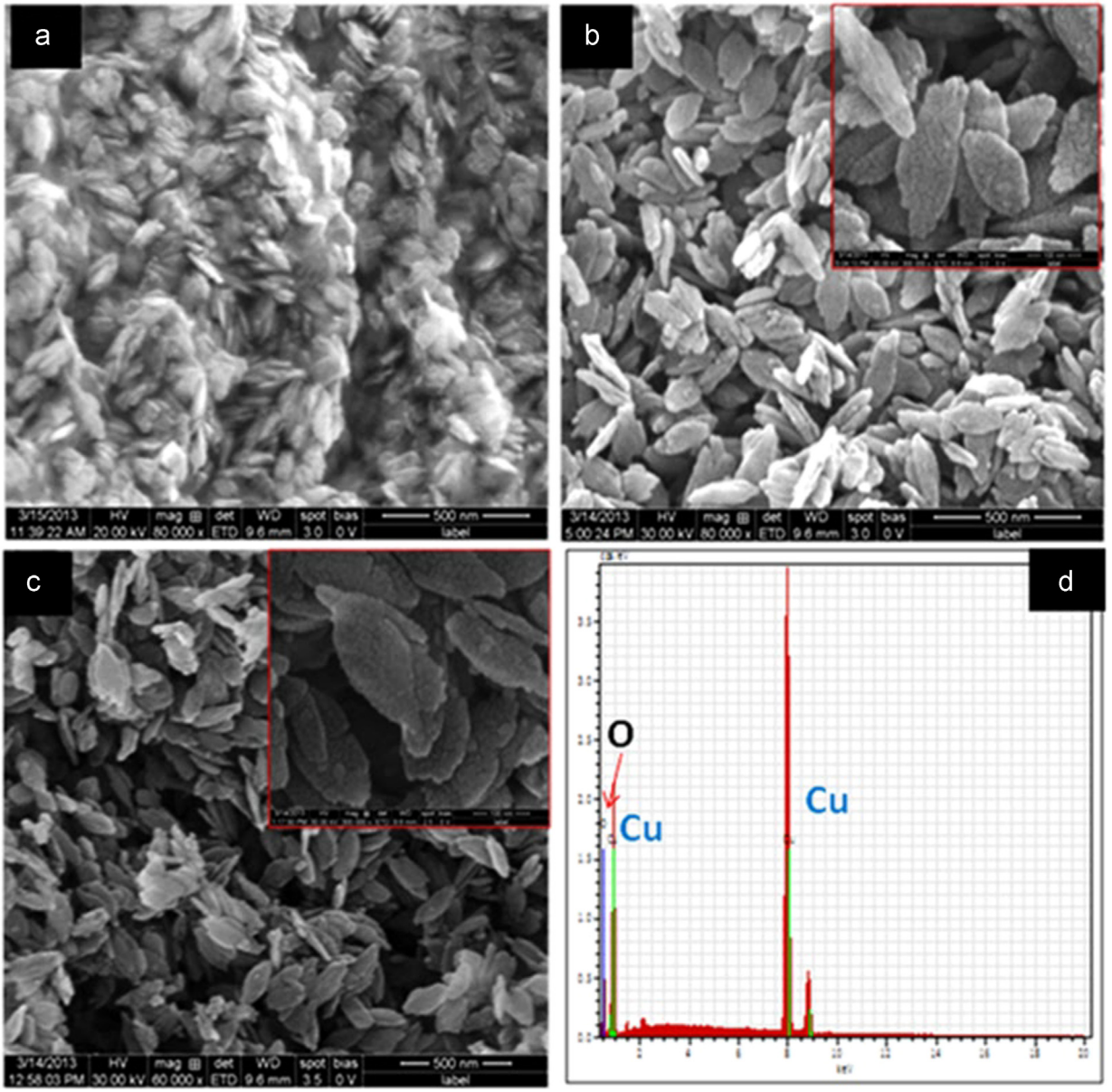

Fig. 2. FESEM images of copper oxide (CuO) nanoleaves: (a) without sodium citrate, (b) with 0.05 M sodium citrate, (c) with 0.1 M sodium citrate, and (d) energy-dispersive X-ray (EDX) spectra of CuO nanoleaves.

length 50–100 nm obtained by the hydrothermal process without citrate, whereas the leaf-like CuO nanostructures (Fig. 2b) with length of 150–200 nm were formed with 0.05 M citrate. On increasing the concentration of citrate to 0.1 M, CuO nanoleaves (Fig. 2c) with a width of 50–100 nm and length of 250–300 nm were formed. A previous report [21] has demonstrated that capping agents can modulate the kinetic growth and determine the subsequent morphologies of the final products.

To further confirm the structure of CuO nanoleaves TEM analysis was carried out. Fig. 3a shows the TEM images of CuO nanoleaves which accords well with the FESEM results, exhibiting leaf-like morphology. The TEM analysis also shows that the size of the nanoleaves is in the range of 250–300 nm. The sizes of the nanoleaves were confirmed by a particle size analyzer and were found to be consistent with the TEM results. The size of the CuO nanoleaves was around 332 nm (Fig. 3c). Selected area diffraction (SAED) pattern (Fig. 3b) demonstrates the polycrystalline nature of the prepared CuO nanoleaves. The diffraction rings in the SAED pattern could be the index to the monoclinic phase with lattice spacing values of 2.7207, 2.5142 and 2.2836 Å for the planes (110), (002) and (111) respectively.

The reaction of $Cu(CH_3COO)_2 \cdot 2H_2O$ in the presence of sodium citrate gives CuO nanoleaves which indicates the key role of sodium citrate in the formation of nanoleaves. A schematic illustration of the formation of CuO

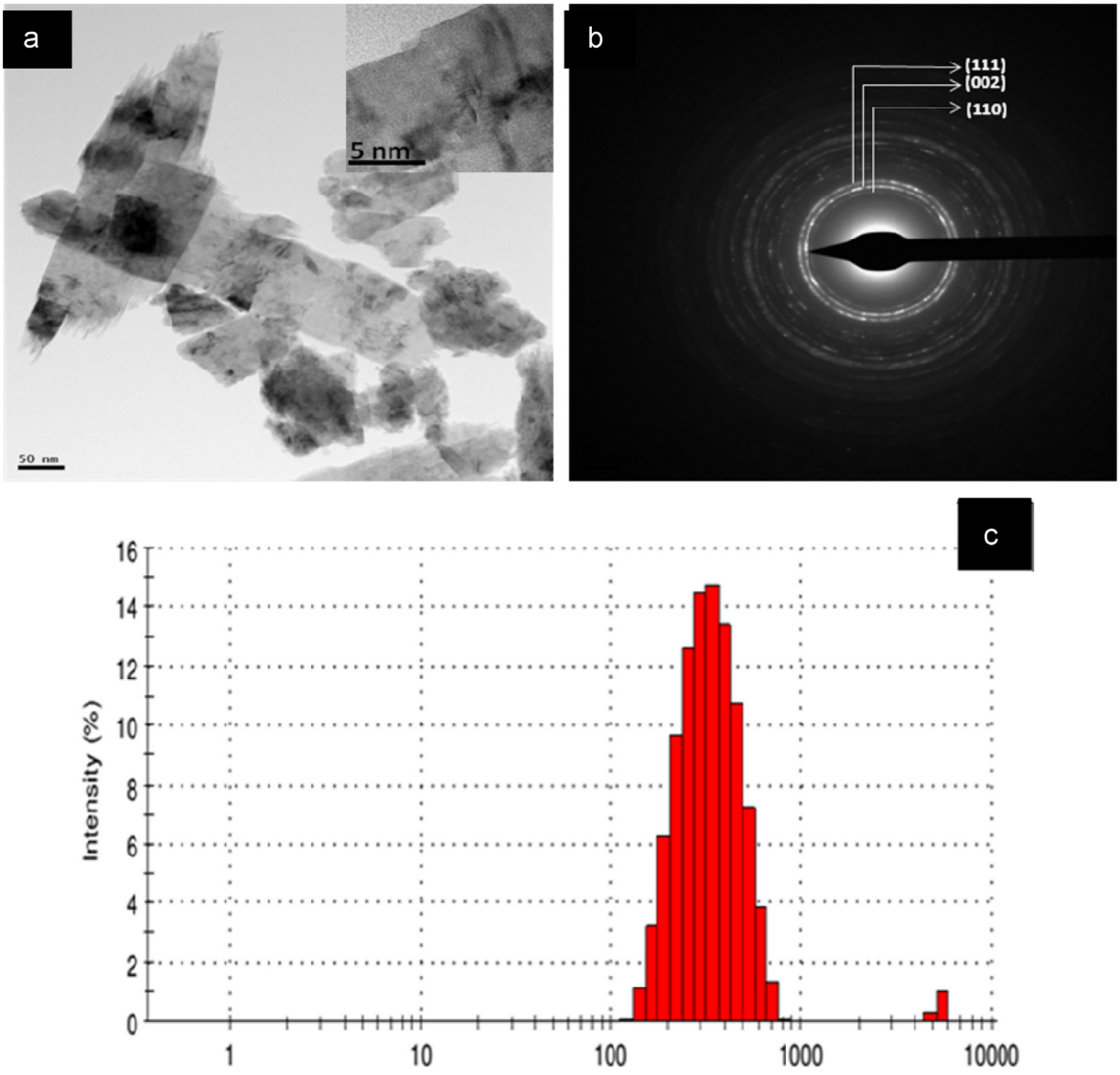

Fig. 3. (a) TEM image of CuO nanoleaves, (b) SAED pattern of CuO nanoleaves and (c) particle size analysis of CuO nanoleaves.

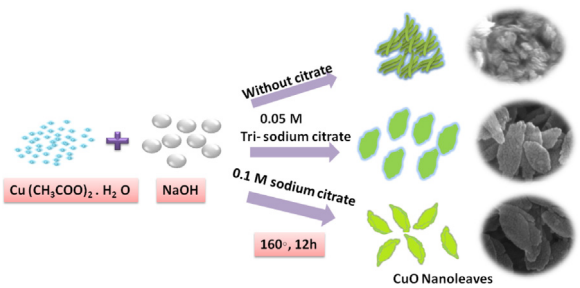

Fig. 4. Schematic illustration of formation of CuO nanoleaves.

nanoleaves is shown in Fig. 4. With the addition of sodium citrate as a structure directing reagent, Cu^{2+} and sodium citrate form a complex and the absorbed citrate on the surface of the $Cu(OH)_2$ nanoparticles slows down the phase transformation as well as the aggregation of CuO nanoparticles [22] leading to the initial formation of leaf-like morphologies (Fig. 2b). On further increasing the content of citrate in the reaction system, more citrate molecules are absorbed on the surface of the $Cu(OH)_2$ nanoparticles, further impeding the phase transformation and decreasing their surface energy, leading to the formation of CuO nanoleaves (Fig. 2c). The chemical composition of the nanoleaves was analyzed by energy dispersive X-ray spectroscopy (EDS) and the spectrum is shown in Fig. 2d, which reveals that the nanoleaves are composed of Cu and O only, and the atomic ratio of Cu to O was very close to 1:1 ratio, which is in agreement with the stoichiometric proportion of CuO.

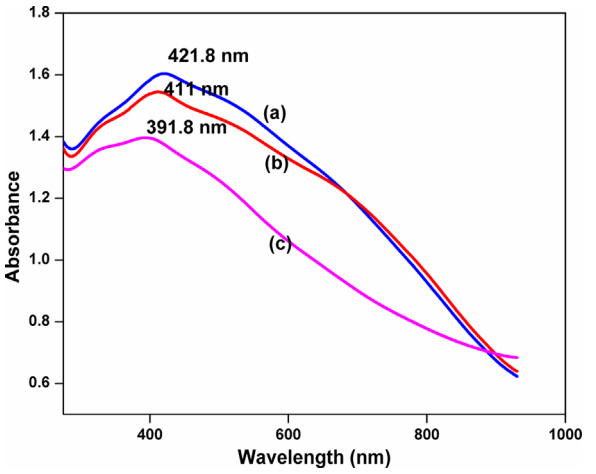

Fig. 5. Absorption spectra of copper oxide (CuO) nanoleaves: (a) without sodium citrate, (b) with 0.05 M sodium citrate and (c) with 0.1 M sodium citrate.

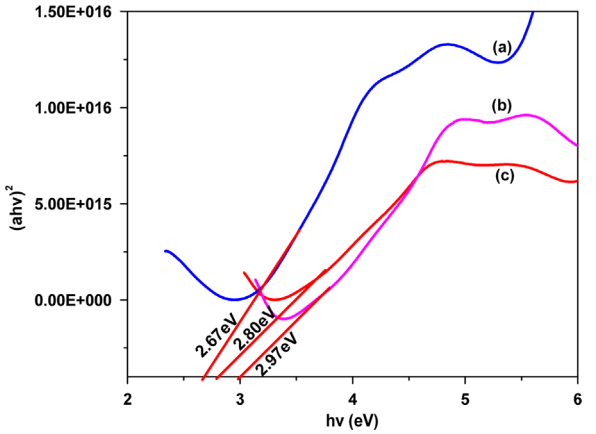

Fig. 6. Plot of $(\alpha h\nu)^2$ vs $h\nu$ of copper oxide (CuO) nanoleaves: (a) without sodium citrate, (b) with 0.05 M sodium citrate and (c) with 0.1 M sodium citrate.

3.3. Optical and surface properties

Light absorption and movement of photogenerated electrons and holes are the major factors in controlling a photocatalytic reaction [23]. The absorption spectra of copper oxide nanoparticles prepared with and without citrate are shown in Fig. 5a–c. Broad absorption peaks are observed at 421.8 nm, 411 nm and 391.8 nm respectively for the three samples revealing the high absorption nature of the spectrum. The optical band gap energy (E_g) of the CuO nanoleaves was estimated as

$$\alpha(E_{photon}) = K(E_{photon} - E_g)^{1/2} \quad (1)$$

where α is the absorption coefficient, E_{photon} is the discrete photon energy, K is a constant, and E_g is the band gap of the material. The band gaps of the three samples can be obtained by plotting $(ah\nu)^2$ vs $h\nu$ in the high absorption range followed by extrapolation of the linear portion of the absorption edge to find the intercept on the X-axis as shown in Fig. 6a–c. The bandgap of the CuO nanoleaves increases from 2.67 to 2.97 eV when the crystallite size of the nanoleaves decreases (Fig. 6). This is due to the quantum confinement effect which arises in semiconducting nanostructures. The band structure changes from the continuous band to discrete energy levels [24].

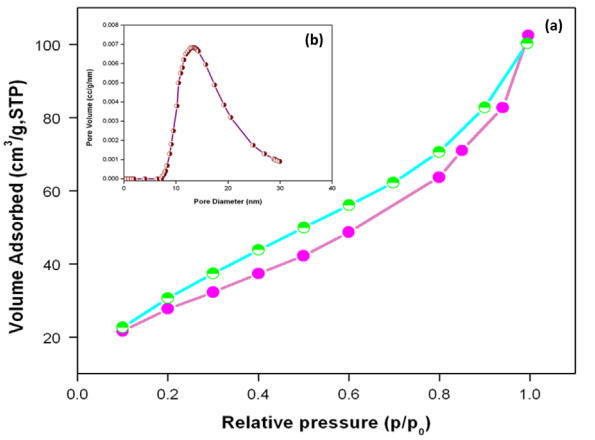

Fig. 7. (a) N_2 adsorption–desorption isotherms and (b) corresponding pore size distribution of the CuO nanoleaves.

The specific surface area of the leaf-like CuO nanostructures was 48.370 $m^2\,g^{-1}$ (Fig. 7). The pore size distribution was calculated by using the Barret–Joyner–Halenda (BJH) method and revealed that the pore sizes of CuO particles were approximately between 2 and 50 nm. This CuO catalyst containing mesopores provides a more efficient corridor for the reactant molecules to shift toward the surface's active sites [25]. Therefore the nanostructured leaf-like CuO photocatalyst can offer a favorable environment for the diffusion and separation of photo-excited electron–hole pairs.

4. Photocatalytic activity of CuO

The organic dyes (MB and MV) were used as the probe molecules to evaluate the photocatalytic performance of the CuO nanostructures in response to ultraviolet light at room temperature. Fig. 8 shows the absorption spectra of methylene blue and methylene violet in the presence of the CuO photocatalyst (prepared at 0.1 M of citrate) for various UV irradiation times. It visibly shows that the absorption peaks of the MB and MV are at 665 nm and 586 nm respectively, diminishing gradually as the exposure time increases from 0 to 3 h. The degradation efficiency ($\eta\% = (1 - A/A_0) \times 100$) for the CuO nanostructures with MB and MV is shown in Fig. 9. The highest degradation rate was observed for CuO nanoleaves prepared with 0.1 M citrate, and the efficiency values were 89% and 96% respectively for MB and MV (Fig. 9).

The preferred degradation was achieved due to the small particle size with large surface area of the CuO particles, which shortens the route for the drift of the photo-induced electron–hole pairs towards the surface of the catalyst to form more active centers. Furthermore, the large surface to volume ratio of the nanoparticles hinders the recombination of photogenerated charge carriers and results in higher photocatalytic efficiency [26]. Commercial CuO (HIMEDIA, 99%) was also

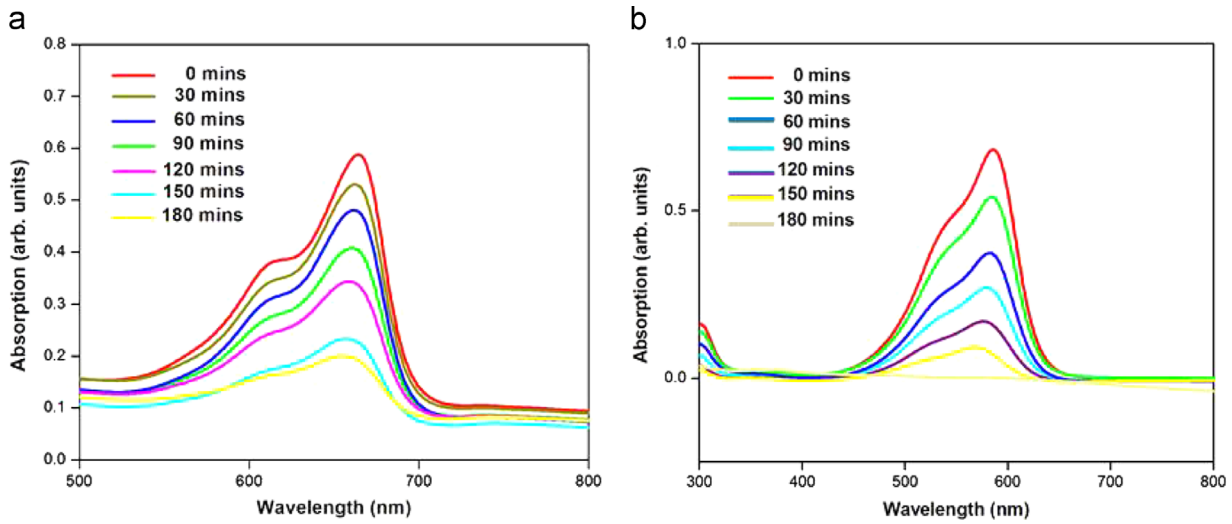

Fig. 8. Photo-degradation of CuO nanoparticles of two organic dyes: (a) MB and (b) MV.

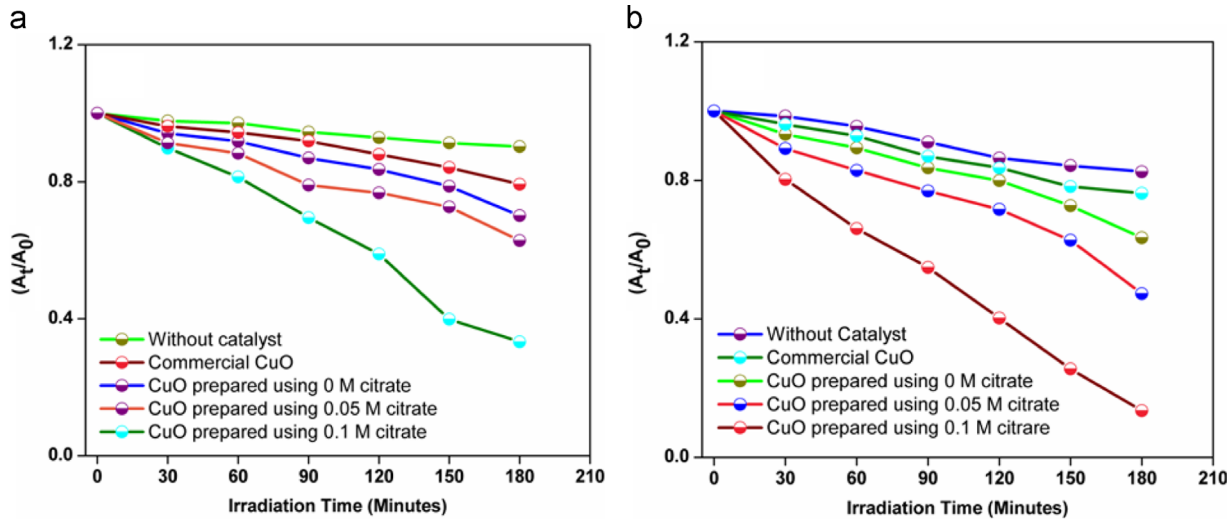

Fig. 9. Degradation efficiency of two organic dyes by the CuO nanostructures under UV irradiation: (a) methylene blue and (b) methylene violet.

used as a reference to evaluate the photocatalytic performance of the synthesized CuO nanostructures. Fig. 9 clearly indicates that the degradation of MB and MV using CuO nanostructures is more rapid than with commercial CuO.

The photocatalytic reaction can be proposed as follows:

$$CuO + h\nu \rightarrow CuO\ (e_{cb}^{-} + h_{vb}^{+})$$

$$H_2O \rightarrow OH^{-} + H^{+}$$

$$h_{vb}^{+} + OH_{ads}^{-} \rightarrow OH$$

$$OH + Dye + O_2 \rightarrow \text{degradation products.}$$

Reuse is one of the most important factors to prove the reproducibility of the photocatalyst. In order to examine the stability of CuO nanoleaves, four cycles of photodegradation experiments were carried out using the same CuO nanoleaves under the same conditions. XRD analysis of CuO after the reaction for four cycles (Fig. 10a) clearly indicates that the material (CuO) was relatively stable and no phase change occurred. After four cycles of photocatalytic reaction, the CuO exhibits a stable photocatalytic activity with small loss as shown in Fig. 10b. This evidently shows that the synthesized CuO is a chemically stable material.

5. Conclusion

In the present study, highly stable CuO nanoleaves were prepared by the simple hydrothermal process and their photocatalytic activity was examined for the degradation of the organic dyes methylene blue and methylene violet in aqueous solution. The XRD analysis confirms the monoclinic structure of CuO with crystallite size varying from 13 nm to 17 nm with variation in reaction conditions. The prepared CuO had excellent photocatalytic properties

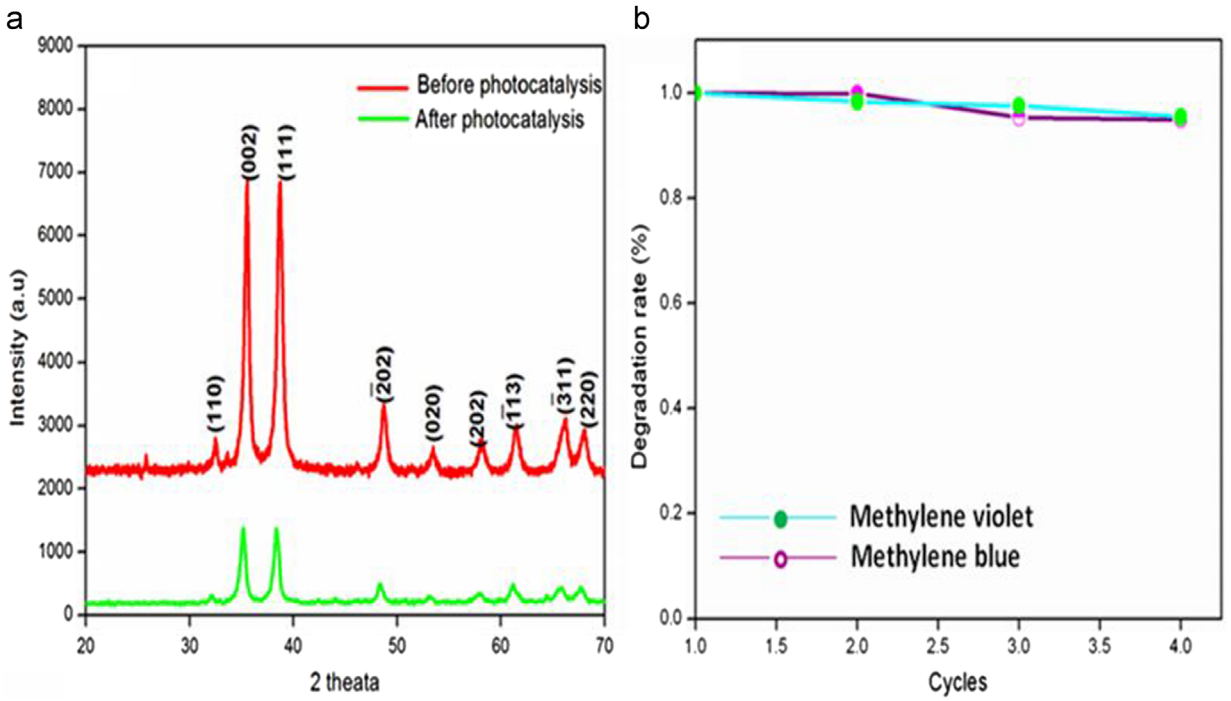

Fig. 10. (a) XRD pattern of CuO nanoleaves before and after use for photocatalytic reaction of four cycles and (b) degradation rate of methylene blue and methylene violet in four cycles.

and the degradation efficiency values of the nanoparticles on methylene blue and methylene violet in the UV region were found to be around 89% and 96% respectively.

Acknowledgment

The authors acknowledge the TEM facilities extended by NIT Trichy under the DST-Nanomission.

References

[1] V. Vamathevan, R. Amal, D. Beydoun, G. Low, S. McEvoy, J. Photochem. Photobiol. A: Chem. 148 (2002) 233–245.
[2] J.B. Reitz, E.I. Solomon, J. Am. Chem. Soc. 120 (1998) 11467–11471.
[3] M. Zhu, G. Dio, Catal. Sci. Technol. 2 (2012) 82–84.
[4] R. Srivastava, M.U.A. Prathap, R. Kore, Colloids Surf. A: Physicochem. Eng. Asp. 392 (2011) 271–282.
[5] X.M. Song, J.M. Wu, M. Yan, Thin Solid Films 517 (2009) 4341–4347.
[6] M. Vijay, V. Selvarajan, K.P. Sreekumar, J. Yu, S.W. Liu, P.V. A. Padmanabhan, Sol. Energy Mater. Sol. Cells 93 (2009) 1540–1549.
[7] A. Mclaren, T.V. Solis, G. Li, S.C. Tsang, J. Am. Chem. Soc. 131 (2009) 12540–12541.
[8] J. Liu, J. Jin, Z. Deng, S. Huang, Z. Hu, L. Wang, C. Wang, L. Chen, Y. Li, G.V. Tendeloo, B. Su, J. Colloid Interface Sci. 384 (2012) 1–9.
[9] Y. Fan, R. Liu, W. Du, Q. Lu, H. Pang, F. Gao, J. Mater. Chem. 22 (2012) 12609–12613.
[10] R. Sahay, J. Sundaramurthy, P.S. Kumar, V. Thavasi, S.G. Mhaisalkar, S. Ramakrishna, J. Solid State Chem. 186 (2012) 261–267.
[11] M. Villani, A.B. Alabi, N. Coppede, D. Calestani, L. Lazzarini, A. Zappettini, Cryst. Res. Technol. 49 (2014) 594–598.
[12] J. Huang, F. TangC. GuC. ShiM. Zhai, Front. Optoelectron. 5 (2012) 429–434.
[13] A. Gu, G. Wang, X. Zhang, B. Fang, Bull. Mater. Sci. 33 (2010) 17–20.
[14] S. Wang, H. Xu, L. Qian, J. Wang, Y. Liu, W. Tang, J. Solid State Chem. 182 (2009) 1088–1093.
[15] Y. Zhang, S. Wing, X. Wang, T. Cui, W.Y. Zhang, Z. Zhang, Eur. J. Inorg. Chem. 1 (2009) 168–173..
[16] M. Zhu, G. Diao, Catal. Sci. Technol. 2 (2012) 82–84.
[17] H. Li, H. Xia, D. Wang, X. Tao, Langmuir 29 (2013) 5074–5079.
[18] J.B. Liang, J.W. Liu, Q. Xie, S. Bai, W.C. Yu, Y.T. Qian, J. Phys. Chem. B 109 (2005) 9463–9467.
[19] H. Xiao, S. Fu, L. Zhu, Y. Li, G. Yang, Eur. J. Inorg. Chem. 56 (2007) 1966–1971.
[20] W.L. Suchanek, R.E. Riman, Adv. Sci. Technol. 45 (2006) 184–193.
[21] Y. Peng, A.W. Xu, B. Deng, M. Antonietti, H. Colfen, J. Phys. Chem. B 110 (2006) 2988–2993.
[22] Y. Li, X.Y. Yang, J. Rooke, G. Van Tendeloo, B.L. Su, J. Colloid Interface Sci. 348 (2010) 303–312.
[23] A. Singhal, M.R. Pai, R. Rao, K.T. Pillai, I. Lieberwirth, A.K. Tyagi, Eur. J. Inorg. Chem. 14 (2013) 2640–2651.
[24] H.M. Xiong, R.Z. Ma, S.F. Wang, Y.Y. Xia, J. Mater. Chem. 21 (2011) 3178–3182.
[25] Yu Xin Zhang, Ming Huang, Fei Li, Zhong Quan Wen, Int. J. Electrochem. Sci. 8 (2013) 8645–8661.
[26] L.J. Wang, Q. Zhou, Y. Liang, H. Shi, G. Zhang, B. Wang, W. Zhang, B. Lei, W.Z. Wang, Appl. Surf. Sci. 271 (2013) 136–140.